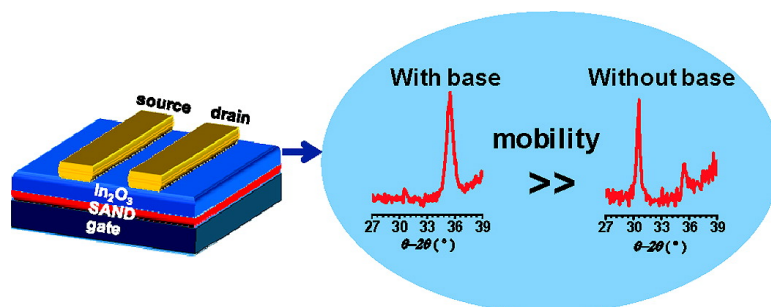Communication

High Performance Solution-Processed Indium Oxide Thin-Film Transistors

Hyun Sung Kim, Paul D. Byrne, Antonio Facchetti, and Tobin J. Marks

More About This Article

Additional resources and features associated with this article are available within the HTML version:

- Supporting Information
- Links to the 2 articles that cite this article, as of the time of this article download
- Access to high resolution figures
- Links to articles and content related to this article
- Copyright permission to reproduce figures and/or text from this article

View the Full Text HTML

High Performance Solution-Processed Indium Oxide Thin-Film Transistors

Hyun Sung Kim, Paul D. Byrne, Antonio Facchetti,* and Tobin J. Marks*

Department of Chemistry and Materials Research Center, Northwestern University, 2145 Sheridan Road, Evanston, Illinois 60208

Received June 11, 2008; E-mail: t-marks@northwestern.edu

Metal oxide electrical properties span a vast range from metallic, to semiconducting, to insulating, all of which are essential characteristics for thin-film transistor (TFT) components.[1] The attraction of metal oxide semiconductors includes high carrier mobilities, wide band gaps, broad transparency windows, tunable doping levels, and amenability to room-temperature film growth. So far, however, metal oxide-based TFTs are far from optimum, with the majority of reported devices fabricated by vapor-phase deposition of the component layers.[2] Low-pressure growth processes are expensive to scale for large areas and high throughput, while solution-phase processes such as printing, spin-coating, dip-coating, electrophoresis, and roll-coating offer promising device fabrication alternatives.[3] Nevertheless, the metal oxide TFTs fabricated to date by semiconductor solution deposition techniques have generally exhibited marginal performance, i.e., low field-effect mobilities, low I_{on}/I_{off} ratios, and large operating voltages, all of which preclude practical application. Note also that, in these TFTs, the gate dielectrics were not solution-processed.

Among metal oxides, In_2O_3 is a promising n-type semiconductor having a wide band gap (3.6−3.75 eV), high single crystal mobility (160 cm^2/V s), and good visible region transparency (>90%).[4] High-quality In_2O_3 thin films are currently grown by low-pressure physical vapor deposition processes,[5] as in high-performance transparent TFTs fabricated at 25 °C by ion-assisted deposition (IAD).[6] These hybrid TFTs combine the excellent semiconducting properties of In_2O_3 with a solution-processed, robust, high-k organic self-assembled nanodielectric (SAND) for the channel and gate dielectric layers, respectively.[7] They exhibit field-effect mobilities as high as 130 cm^2 V^{-1} s^{-1}, $I_{on}/I_{off} = 10^5$, subthreshold gate voltage swing = 190 mV/decade and operate at ~2.0 V.[6] These results raise the question of whether and by which methodology TFT-applicable In_2O_3 films might be grown by simple solution techniques. We report here the first demonstration of solution-processed In_2O_3 TFTs using SiO_2 and SAND as gate dielectrics (Figure 1). We demonstrate that optimized film precursor stoichiometry in combination with the SAND gate dielectrics enables high-mobility In_2O_3 film growth and excellent TFT performance.

In_2O_3 film precursor solutions were prepared with $InCl_3$ as the In^{3+} source and ethanolamine (EAA) as an added base. After some experimentation, the optimal $InCl_3$ concentration was found to be 0.1 M in methoxyethanol (see Table S1), while the EAA/In^{3+} molar ratio was varied systemically from 0.0 to 15. These homogeneous solutions were stirred for 30 min at room temperature and then spin-coated onto SiO_2 (300 nm)- and SAND (~16.5 nm)-coated n^+-Si substrates (TFT gate contact). Next, the spin-coated films were annealed at 400 °C for 10 min in a tube furnace under air (see Supporting Information). This temperature was found to be optimum by X-ray diffraction (XRD) monitoring of the film crystallization process in annealing between 200 and 400 °C (Figure 2A). After annealing, the films were cooled to room temperature, and the spin-coating process was repeated x times ($x = 0 − 4$, depending on the formulation) until the In_2O_3 film thickness which
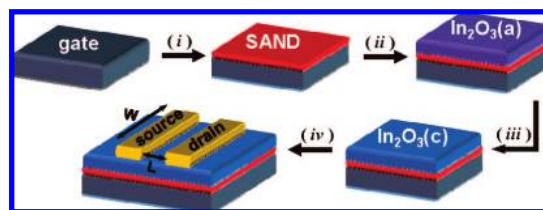

Figure 1. Fabrication of In_2O_3 TFTs on Si-SAND (16.5 nm) substrates. L (channel length) = 50 or 100 μm, W (channel width) = 500 μm.

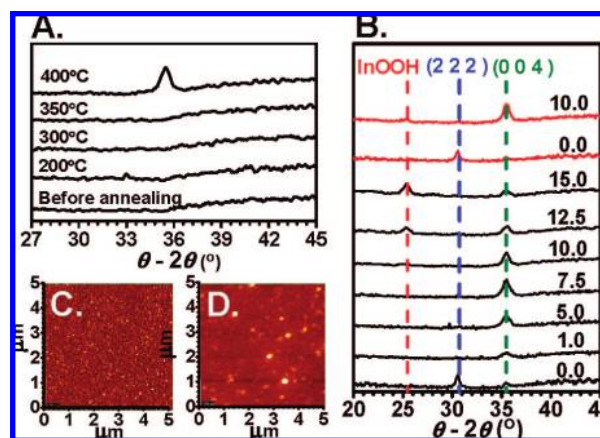**Figure 2.** (A) $\theta-2\theta$ XRD scans of In_2O_3 films grown on Si/SiO_2 substrates and then annealed at the indicated temperatures (EAA/In^{3+} = 10). (B) XRD patterns of In_2O_3 films on Si/SiO_2 (black lines) and Si/SAND (red lines) substrates fabricated from precursor solutions having the indicated EAA/In^{3+} molar ratios and annealed at 400 °C. AFM images of In_2O_3 films grown on Si/SiO_2 (C) and Si/SAND (D); EAA/In^{3+} = 10.

maximized TFT performance (~30 nm, *vide infra*) was achieved. Other work shows that SAND films are stable to such annealing conditions.[8] The TFT structure was completed by Au thermal evaporation through a shadow mask to define the source/drain contacts (Figure 1).

The critical effect of the ethanolamine concentration used in the precursor solutions is evident in the XRD scans of In_2O_3 films shown in Figure 2. Independent of the underlying gate dielectric, the annealed films deposited from base-free formulations are textured but exhibit low carrier mobility and mixed (222) and (004) In_2O_3 reflections. However, as the EAA/In^{3+} molar ratio is increased to 7.5−10, the (222) reflection disappears, and the growth orientation associated with the higher carrier mobility (004)[9] reflection becomes predominant (Figure 2B). Interestingly, when the EAA/In^{3+} molar ratio is increased further (10 → 15), the corresponding films become less crystalline and an additional InOOH (~25°) reflection appears. It will be shown that these microstructural features strongly influence the TFT response.

The morphologies and grain sizes of the present solution-processed In_2O_3 thin films were examined by tapping-mode atomic force microscopy (AFM). Figure 2C and D show that the In_2O_3
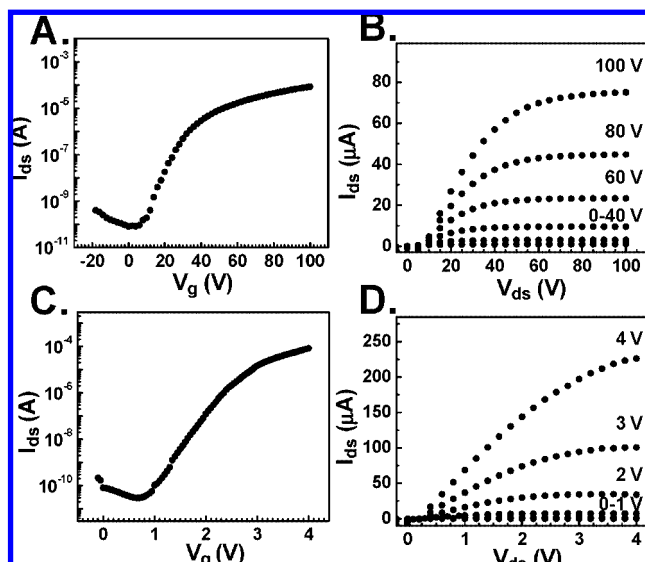
Figure 3. Transfer (A, C) and output (B, D) plots for In₂O₃-based TFTs having the following structures: (A and B) Si/SiO₂ (300nm)/In₂O₃ (30 nm)/Au (50nm), $L = 100$ μm, $W = 1000$ μm. (C and D) Si/SAND (16.5 nm)/In₂O₃ (30nm)/Au (50nm), $L = 100$ μm, $W = 500$ μm.

Table 1. In₂O₃-Based TFT Parameters in Ambient with SiO₂ or SAND as Gate Dielectrics for Semiconducting Films Spin-Coated from the Formulations Having the Indicated EAA/In³⁺ Molar Ratios

EAA/In³⁺	diel.	μ (cm²/V s)[a]	I_{on}/I_{off}	V_{th} (V)	S (V/dec)
0.0	SiO₂	0.04 ± 0.01	10⁴	42.6	23.8
1.0	SiO₂	~0.01	10⁴	44.3	16.0
5.0	SiO₂	0.05 ± 0.01	10⁴	54.2	15.3
7.5	SiO₂	0.12 ± 0.03	10⁴	38.0	11.4
10.0	SiO₂	0.70 ± 0.09	10⁶	29.8	5.7
12.5	SiO₂	0.35 ± 0.05	10⁵	44.6	11.2
15.0	SiO₂	0.22 ± 0.03	10³	36.5	26.0
0.0	SAND	5.50 ± 0.6	10⁴	2.6	0.4
10.0	SAND	43.7 ± 4.8	10⁶	2.2	0.3

[a] Calculated in saturation from the equation $\mu = (2I_{SD}L)/[WC_{OX}(V_{SG} - V_{th})^2]$.

films fabricated on the different dielectrics are compact, dense, uniform, and reasonably smooth (rms roughness ~3 nm on SiO₂, ~6 nm on SAND). These films are less smooth than those reported using the aforementioned vapor-phase deposition processes.[6]

After TFT fabrication, the devices were evaluated in ambient atmosphere. Typical I−V plots are shown in Figure 3, and Table 1 summarizes performance parameters as a function of precursor EAA/In³⁺ molar ratio and dielectric type. Interestingly, as the base/In³⁺ ratio is increased, the mobility tracks the microstructural evolution observed by XRD. In all cases, the greatest mobility is observed for an EAA/In³⁺ molar ratio ~10. For these formulations, the In₂O₃ devices on the SiO₂ gate dielctric exhibit reasonable field-effect responses ($\mu = 0.7$ cm²/V s; $I_{on}/I_{off} = 10^6$) for operating voltages in the 0.0−100 V range. Note that there is an optimal In₂O₃ film thickness (~30 nm) where both the carrier mobility and I_{on}/I_{off} are large (Table S2). Since I_{off} should increase proportionately with semiconductor thickness, we are currently investigating the origin of these unusual effects. In contrast to the SiO₂ results, the In₂O₃−organic hybrid TFTs fabricated with the SAND dielectrics exhibit excellent I−V characteristics (Figure 3C, D) with classical/crisp pinch-off linear curves and saturation at very low operating voltages (0.0−4.0 V). Analysis of the n⁺-Si/SAND/In₂O₃/Au TFT electrical response reveals large saturation-regime field-effect mobilities, up to 43.7 cm² V⁻¹ s⁻¹, $I_{on}/I_{off} = 10^6$, which is

encouraging for high-speed applications at very low operating voltages (0.0−4.0 V).

All of the present solution-processed In₂O₃ films are colorless to the eye and spectroscopically transparent, with films deposited on glass substrates exhibiting an average transparency of ~95% in the visible region (Figure S1A). The optical band gap (3.65 eV) was estimated from the transmittance spectrum by extrapolating the linear part of $(\alpha h\nu)^2$ vs $h\nu$ plots to $\alpha = 0$ (Figure S1B). The transmittance and band gap data suggest that these In₂O₃ thin films are ideal n-channel materials for transparent TFTs.

In conclusion, these results demonstrate that hybrid integration of solution-processed metal oxide semiconductor films with nanoscopic organic dielectrics enables TFTs exhibiting performance unobtainable via conventional approaches. Such hybrid TFT strategies should be applicable to other metal oxide based transistor structures (bottom-contact, top-gate) as well as to other transparent semiconductors and organic dielectric combinations. A key enabler of the present process is an In₂O₃ film precursor formulation with a proper base/In³⁺ molar ratio, which optimizes the semiconductor film microstructure.

Supporting Information Available: Experimental details, field-effect device characteristics of TFTs, figures of In₂O₃ film optical properties. This material is available free of charge via the Internet at http://pubs.acs.org.

References

(1) (a) Sun, Y.; Rogers, J. A. *Adv. Mater.* **2007**, *19*, 1897. (b) Nomura, K.; Ohta, H.; Takagi, A.; Kamiya, T.; Hirano, M.; Hosono, H. *Nature* **2004**, *432*, 488. (c) Sun, B.; Peterson, R. L.; Sirringhaus, H.; Mori, K. *J. Phys. Chem. C* **2008**, *111*, 18831. (d) Ko, S. H.; Park, I.; Pan, H.; Misra, N.; Rogers, M. S.; Grigoropoulos, C. P.; Pisano, A. P. *Appl. Phys. Lett.* **2008**, *92*, 154102. (e) Kim, J. S.; Park, J. H.; Lee, J. H.; Jo, J.; Kim, D.-Y.; Cho, K. *Appl. Phys. Lett.* **2007**, *91*, 112111. (f) Pal, B. N.; Sun, J.; Jung, B. J.; Choi, E.; Andreou, A. G.; Katz, H. E. *Adv. Mater.* **2008**, *20*, 1023.
(2) (a) Ohya, Y.; Niwa, T.; Ban, T.; Takahashi, Y. *Jpn. J. Appl. Phys* **2001**, *40*, 297. (b) Hoffman, R. L.; Norris, B. J.; Wager, J. F. *Appl. Phys. Lett.* **2003**, *82*, 733. (c) Chiang, H. Q.; Wager, J. F.; Hoffman, R. L.; Jeong, J.; Keszler, D. A. *Appl. Phys. Lett.* **2005**, *86*, 013503. (d) Jackson, W. B.; Hoffman, R. L.; Herman, G. S. *Appl. Phys. Lett.* **2005**, *87*, 193503. (e) Görrn, P.; Sander, M.; Meyer, J.; Kröger, M.; Becker, E.; Johannes, H.-H.; Kowalsky, W.; Riedl, T. *Adv. Mater.* **2006**, *18*, 738.
(3) (a) Ong, B. S.; Li, C.; Li, Y.; Wu, Y.; Loutfy, R. *J. Am. Chem. Soc.* **2007**, *129*, 2750. (b) Sun, B.; Sirringhaus, H. *J. Am. Chem. Soc.* **2006**, *128*, 16231. (c) Lee, D-H.; Chang, Y-J.; Herman, G. S.; Chang, C-H. *Adv. Mater.* **2007**, *19*, 843. (d) Cheng, H-C.; Chen, C-F.; Tsay, C-Y. *Appl. Phys. Lett.* **2007**, *90*, 012113. (e) Cho, J. H.; Lee, J.; He, Y.; Kim, B.; Lodge, T. P.; Frisbie, C. D. *Adv. Mater.* **2008**, *20*, 686. (f) Loi, M. A.; Da Como, E.; Dinelli, F.; Murgia, M.; Zamboni, R.; Biscarini, F.; Muccini, M. *Nat. Mater.* **2005**, *4*, 81–85.
(4) (a) Nakazawa, H.; Ito, Y.; Matsumoto, E.; Adachi, K.; Aoki, N.; Ochiai, Y. *J. Appl. Phys.* **2006**, *100*, 093706. (b) Gupta, A.; Cao, H.; Parekh; Rao, K. K. V.; Raju, A. R.; Waghmare, U. V. *J. Appl. Phys.* **2007**, *101*, 09N513.
(5) (a) Zhang, D.; Liu, Z.; Li, C.; Tang, T.; Liu, X.; Han, S.; Lei, B.; Zhou, C. *Nano. Lett.* **2004**, *10*, 1919. (b) Dhananjay; Chu, C-W. *Appl. Phys. Lett.* **2007**, *91*, 132111. (c) Vygranenko, Y.; Wang, K.; Nathan, A. *Appl. Phys. Lett.* **2007**, *91*, 263508. (d) Presley, R. E.; Munsee, C. L.; Park, C-H.; Hong, D.; Wager, J. F.; Keszler, D. A. *J. Appl. Phys. D: Appl. Phys.* **2004**, *37*, 2810. (e) Lavareda, G.; de Carvalho, C. N.; Fortunato, E.; Ramos, A. R.; Alves, E.; Conde, O.; Amaral, A. *J. Non-Cryst. Solids* **2006**, *352*, 2311. (f) Lorenz, H.; Stoger-Pollach, M.; Schwarz, S.; Pfaller, K.; Klotzer, B.; Bernardi, J.; Penner, S. *J. Phys. Chem. C* **2008**, *112*, 918.
(6) (a) Wang, L.; Yoon, M-H.; Facchetti, A.; Marks, T. J. *Adv. Mater.* **2007**, *19*, 3252. (b) Wang, L.; Yoon, M-H.; Lu, G.; Yang, Y.; Facchetti, A.; Marks, T. J. *Nat. Mater.* **2006**, *5*, 893.
(7) Yoon, M-H.; Facchetti, A.; Marks, T. J. *Proc. Natl. Acad. Sci. U.S.A.* **2005**, *102*, 4678.
(8) (a) Byrne, P. D.; Facchetti, A.; Marks, T. J. *Adv. Mater.* **2008**, *20*, 1. (b) Lin, H. C.; Kim, S. K.; Chang, D.; Xuan, Y.; Mohammadi, S.; Ye, P. D.; Lu, G.; Facchetti, A.; Marks, T. J. *Appl. Phys. Lett.* **2007**, *91*, 092103.
(9) Mirzapour, S.; Rozati, S. M.; Takwale, M. G.; Marathe, B. R.; Bhide, V. G. *Mater. Lett.* **1992**, *13*, 275.

JA804262Z